Spectrochimica Acta Part A: Molecular and Biomolecular Spectroscopy 135 (2015) 907–914

Contents lists available at ScienceDirect

Spectrochimica Acta Part A: Molecular and Biomolecular Spectroscopy

journal homepage: www.elsevier.com/locate/saa

Vibrational spectroscopy and conformation of S-ethyl thioacetate: $CH_3COSCH_2CH_3$ and comparison with —C(O)S— and —C(O)O— compounds

María Eliana Defonsi Lestard, María Eugenia Tuttolomondo, Aida Ben Altabef *,[1]

INQUINOA, CONICET, Instituto de Química Física, Facultad de Bioquímica, Química y Farmacia, Universidad Nacional de Tucumán, San Lorenzo 456, T4000CAN Tucumán, Argentina

HIGHLIGHTS

- The molecular geometry and the conformations for the compound have been calculated.
- NBO calculations have been performed in order to explain the preferred conformation.
- The transferability concept is useful to predict the conformational preference.

GRAPHICAL ABSTRACT

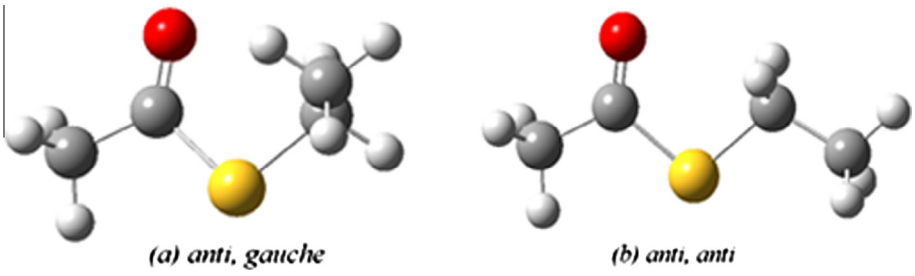

ARTICLE INFO

Article history:
Received 27 May 2014
Received in revised form 4 July 2014
Accepted 17 July 2014
Available online 7 August 2014

Keywords:
S-ethyl thioacetate
Infrared
Raman
—C(O)S— and —C(O)O— compounds

ABSTRACT

The molecular structure and conformational properties of S-ethyl thioacetate, $CH_3COSCH_2CH_3$, were determined in the gas phase by electron diffraction and vibrational spectroscopy (IR and Raman). The experimental investigations were supplemented by *ab initio* (MP2) and DFT quantum chemical calculations at different levels of theory. Theoretical methods reveal two structures with C_s (*anti*, *anti*) and C_1 (*anti*, *gauche*) symmetries. The infrared and Raman spectra for different phases were also recorded and the bands observed assigned to the vibrational normal modes. Liquid Raman and infrared spectra in liquid and gaseous state measurements revealed the presence of two conformations *anti*, *anti* (C_s symmetry) and *anti*, *gauche* (C_1 symmetry).

The study was completed using natural bond orbital (NBO) analysis. We have also analyzed the internal rotation barrier about the C(O)SCC dihedral angle using a variety of computational approaches and natural bond orbital (NBO) analyses to understand the nature of the potential function and to explain the preferred conformation of the molecule.

Introduction

S-ethyl thioacetate, $CH_3COSCH_2CH_3$, is an acetylating agent used to provide an amine-protecting group [1]. Thioesters such as $CH_3COSCH_2CH_3$ are also important components of coenzyme A, which plays an essential role in metabolism [2]. The different reactivity of thioesters as compared to that of oxoesters has attracted considerable interest in the past years. The molecular structure of S-methyl thioacetate, $CH_3C(O)SCH_3$, was determined by gas electron diffraction (GED) [3], though notably the existence was found of only one stable conformer of the title molecule; a structure with syn conformation (C=O double bond syn with respect to the S—C(H_3) single bond. Teixeira-Dias et al., studied the nature and relative importance of intramolecular interactions involving both the —CH(CH,), and the HC(=X)Y (X,Y = 0 or S) [4]. Rui Fausto et al. studied the conformational preferences and

* Corresponding author. Tel.: +54 381 4311044; fax: +54 381 4248169.
E-mail address: altabef@fbqf.unt.edu.ar (A. Ben Altabef).
[1] Member of the Carrera del Investigador Científico, CONICET, Argentina.

http://dx.doi.org/10.1016/j.saa.2014.07.054
1386-1425/

vibrational properties of cis- and trans-s-ethyl thiocrotonate by a combined *ab initio* SCF-MO calculation and vibrational spectroscopic approach, as a first step to the general understanding of the conformational and vibrational properties of α, β unsaturated thioesters [5].

Although the structural and conformational properties of simple oxoesters and thioesters have been studied by several groups, mainly because of the central role of thioesters in the metabolic process, the factors controlling this behavior are far from being understood. This was highlighted in an extensive computational study undertaken by Drueckhammer et al. [6]. The role played by experimental structural studies in understanding the behavior of molecules has been recently discussed [7], and gas electron diffraction (GED) has already been used to determine the structures of many —SC=O— containing compounds. In addition to the early work of Shen and Hagen on ClC(O)SCl [8], the GED group of Oberhammer et al. has reported gas-phase structures for several related species [9–14].

Structural information from GED diffraction studies of various esters with the general formula $CF_3C(O)R$ [15–18], (R = SCH_2CH_3, OCH_3, OCH_2CH_3, OCH_2CF_3) revealed the preference of the *anti*, *anti* and *anti*, *gauche* structure; a starting point in structural analysis would be that thioesters in general are most stable in the *anti*, *anti* and *anti*, *gauche* conformations as evidenced by the structural information transferability from these esters. The transferability concept is very useful to predict the structure and conformational preference of the S-ethyl thioacetate by means of quantum mechanical calculations and vibrational analysis.

Raman and infrared spectra in liquid and gaseous state measurements revealed the presence of two conformations *anti*, *anti* (C_s symmetry) and *anti*, *gauche* (C_1 symmetry). The experimental measurements were complemented by quantum chemical calculations to obtain and optimize molecular structure and wavenumbers corresponding to the normal modes of vibration. We have also analyzed the internal rotation barrier about the C(O)SCC dihedral angle using a variety of computational approaches and natural bond orbital (NBO) analyses to understand the nature of the potential function and to explain the preferred conformation of the molecule.

Material and methods

Experimental

A sample of $CH_3COSCH_2CH_3$ for use in both diffraction and spectroscopy experiments were purchased from Sigma–Aldrich and used without further purification. Its purity was confirmed by FTIR spectroscopy.

Infrared and Raman spectroscopy

Infrared spectra of $CH_3COSCH_2CH_3$ in the gas and liquid phase were recorded in the 4000–400 cm^{-1} range at room temperature using a Perkin-Elmer GX1 FTIR instrument. A glass cell with a 10 cm optical path and KBr windows were used.

The Raman spectrum of the liquid at room temperature was obtained with an FT-Raman RFS 100/S spectrometer using a 1064 nm line from a Nd:YAG laser for excitation.

Computational details

Calculations were performed using the Gaussian 03 suite of programs [19]. Potential-energy curves were calculated with the MP2 [20], mPW1Pw91 [21] and B3LYP [22–24] methods in combination with the 6-311++G(d,p) [25] basis. Fig. 1 shows the rotational barriers of the S—C(H2) bond (C(16)S(28)C(21)C(24) dihedral angle) at

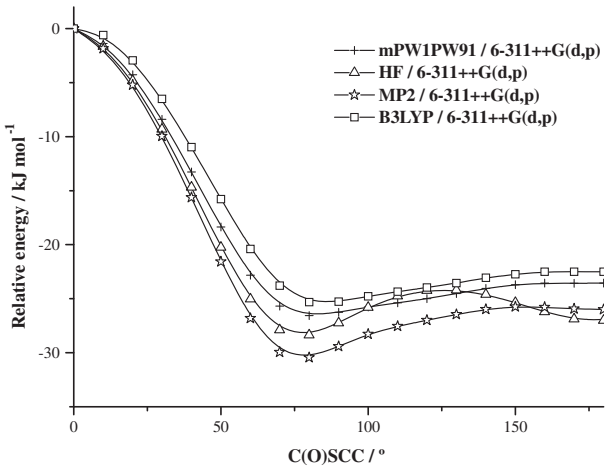

Fig. 1. Torsional potential curves about the S—C(H_2) bond of $CH_3COSCH_2CH_3$ calculated at different levels of calculations.

different levels of theory. All calculations were performed in such ways that only the given torsion was fixed and all other parameters were allowed to relax. The total energy curve was constructed in steps of 10° using default convergence criteria as implemented in Gaussian 03.

Two minima were identified by rotating about the S—C(H_2) bond, the global minimum representing a C_1-*symetric* (*anti*, *gauche*) (Fig. 2a) structure and another, higher in energy, representing a C_s-*symmetric* (*anti*, *anti*) (Fig. 2b).

Geometry optimizations were first performed for both conformers at the MP2 and B3LYP methods with the 6-31G(d), 6-311G(d,p) basis set and at B3LYP/6-311G++(d,p) combination. One the DFT methods used Becker's B3 [21] hybrid exchange functional and the Lee–Yang–Parr non-local correlation functional (LYP) [22]. All calculations were spin-restricted and frozen-core.

Natural bond orbital (NBO) [23] calculations were performed at the B3LYP/6-311G++(d,p) level using the NBO 3.0 code as implemented in the Gaussian 03 package.

Results and discussion

Quantum chemical calculations

As expected, the calculation showed two stable conformations with C_1 (*anti*, *gauche*) and C_s (*anti*, *anti*) symmetries at every combination of level of theory and basis set used. In the *anti*, *gauche* conformations (two enantiomeric forms) the C(15)C(16)S(28)C(21) dihedral angles are 180°, while the C(16)S(28)C(21)C(24) dihedral angle has a *gauche* value of approximately +/−79 and +/−86° depending on the level of calculation (Fig. 2a). In the *anti*, *anti* conformation the C(15)C(16)S(28)C(21) and C(16)S(28)C(21)C(24) dihedral angles are both 180° (Fig. 2b).

Calculated geometrical parameters for $CH_3COSCH_2CH_3$ are listed in Table S1 for both conformers. As found for the related compound $CF_3C(O)SCH_2CH_3$ [15] and $CH_3SO_2SCH_3$ [25], $CF_3SO_2SCF_3$ [26], $CF_3SO_2CF_3$ [27] the inclusion of extra polarization functions (beyond a single d function) is necessary to predict the bond lengths in this type of molecule accurately.

As there were no geometrical experimental data for this molecule, the information obtained for $CF_3C(O)SCH_2CH_3$ [15] was considered and an extrapolarization function was included to predict more accurately the geometric parameters involving the S atom. When replacing the 6-311G(d,p) [28] by 6-311G(3df,3pd) [29,30] basis set in the calculation all S—C bonds suffer a shortening of

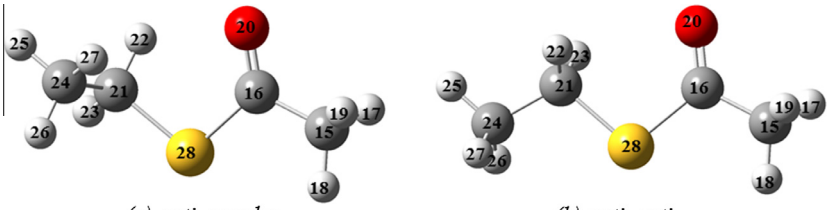

Fig. 2. Molecular structure of the $CH_3C(O)SCH_2CH_3$: *a- anti, gauche* and *b- anti, anti* conformers calculated at the B3LYP76-311++G(d,p) level.

approximately 1.5 pm while the other bonds remain without significant changes.

The two minima were optimized using different methods. From these calculations the free energy values of each conformer could be obtained and the relative population of both conformers was calculated using the Boltzman distribution equation (Table 1).

It is interesting to observe how the C_s conformer proportion predominates according to all calculations performed with the exception of the one carried out at the B3LYP/6-311++G(d,p) level which indicates that the population ratio between the two geometries is close to the unit. This behavior was observed and studied for the $CF_3C(O)SCH_2CH_3$ [15], where the results of calculation with the best level were close to those measured experimentally by GED.

Fourier decomposition

The study of the nature of the barrier of C(O)SCC torsion in terms of hyperconjugative, steric, and electrostatic interactions will give us an insight into the reasons for the relative stability of the two conformers. The potential energy surface for the target torsion angle was calculated in 10 steps in the 0–180° allowing all other geometrical parameters to relax. The energy profiles were fitted to the sixth-order Fourier expansion [31–34].

$$V(\theta) = \sum_{i=1}^{6} \frac{1}{2} V_{iN}(1 - \cos iN\theta)$$

where N, the symmetry number, is equal to 1. No contributions to torsional energies from zero-point energy were taken into account.

The decomposition of the total energy function and the analysis of the different V_i terms have previously been shown to be an effective method of analyzing the stabilization of the different molecular system conformations. Table S1 lists the six V_i terms calculated for $CH_3COSCH_2CH_3$ using different methods. With their large values, V_1 and V_2 are the main contributions to the rotational barrier with $V_1 > V_2 > V_3$. V_{4-6} are less significant when deconvoluting the potential energy curve. The magnitudes and signs of the two main terms are similar regardless of the level of theory used to calculate them. V_2 is usually associated with conjugative and hyperconjugative effects that have a periodicity of 180°. As for V_1, it usually accounts for interactions between local dipoles and for steric interactions. The V_3 term is associated with unfavorable bond–bond eclipsing interactions, exhibiting a threefold periodicity for a torsion involving sp^3-hybridized sulfur atoms [34].

In Fig. 3 the Fourier decomposition of the potential energy function with respect to the $C(sp^2)(O)SC(sp^3)C(sp^3)$ C(O)SCC dihedral angle is presented. V_1 is large and negative showing that there is a strong preference for an *anti anti* geometry. This fact can be rationalized by considering the interactions between the local dipole of the $C(O)CH_3$ group and the SCH_2CH_3 group. V_2, related to hyperconjugative interactions and is responsible for the *anti*, *gauche* conformer. The V_3 term is associated with unfavorable bond–bond eclipsing interactions, exhibiting a 3-fold periodicity for a torsion involving sp^3-hybridized sulfur atom.

NBO analysis

The NBO analysis has often been used in the evaluation of the anomeric effect to explain the origin of the internal rotational barrier. The NBO [24] analysis is used us to estimate the energy of the molecule with the same geometry but in the absence of electronic delocalization. Moreover, only the steric and electrostatic interactions through E_{Lewis} are taken into account:

$$\Delta E_{barrier} = \Delta E_{Lewis} + \Delta E_{deloc} \quad (1)$$

ΔE_{Lewis} represents the energy of the hypothetical localized species described by a determinant of nearly doubly occupied NBOs comprising the core electrons, lone pairs and localized bonds of the Lewis structure; and the delocalization energy change ΔE_{deloc} represents the hyperconjugative stabilization contribution to the rotational barrier that arises from bond → antibond charge transfer.

An NBO calculation was therefore performed on $CH_3C(O)SCH_2CH_3$ for both C_s and C_1 conformers at the B3LYP/6-311++G(d,p) level of theory.

It is interesting to observe that the electrostatic and steric contributions tend to favor the *anti*, *anti* conformer, whereas the delocalization contribution tends to favor the *anti*, *gauche* conformer, as expected from the anomeric effect (Table S2).

Table 2 reports the most important hyperconjugative interaction contributions. The favoring of the *anti*, *gauche* conformer is mainly due to the lp [S → σ*C(21)—C(24)] and lp [S → σ*C(24)—H(26,27)] interactions.

In order to confirm the contribution of the different terms in the Fourier decomposition, we performed an investigation of the energy barrier based on the partition offered by the equation:

Table 1
Free energies (G) difference in free energies (ΔG) for C_1 and C_s conformers and population ratio of $CH_3C(O)SCH_2CH_3$ calculated at different levels of theory.

		$G(C_1)$[a]	$G(C_s)$	ΔG [b]	C_1:C_s
B3LYP	6-31G(d)	−630.587113	−630.587407	0.77	60:40
	6-311G(d.p)	−630.682295	−630.682076	0.77	60:40
	6-311++G(d.p)	−630.688387	−630.689001	1.61	51:49
MP2	6-31G(d)	−629.248716	−629.248366	−0.92	74:26
	6-311G(d.p)	−629.434336	−629.433420	−2.41	88:22

[a] Energies in Hartrees.
[b] $\Delta G = G(C_1) - G(C_s)$ in kJ mol^{-1}.

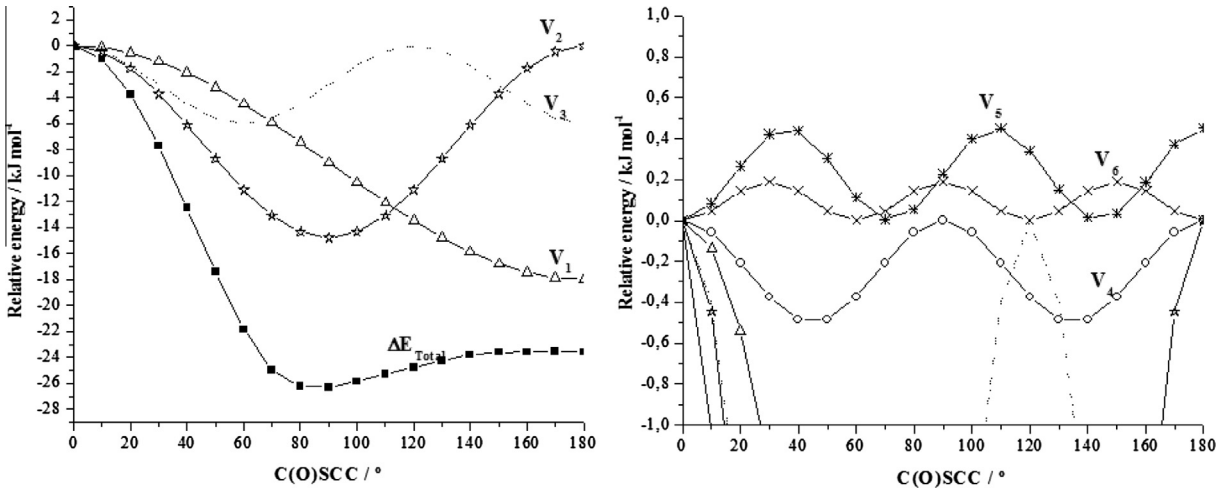

Fig. 3. Fourier decomposition of potential function $V(\phi)$ for $CH_3C(O)SCH_2CH_3$ calculated using B3LYP with 6-311++G(d,p) basis set. On the right is an enlargement of the region containing V_4, V_5 and V_6.

Table 2
Important hyperconjugative interactions in kJ mol^{-1} for $CH_3C(O)SCH_2CH_3$ calculated at B3LYP/6-311++G(d,p) level.

	anti, gauche ϕ C(O)SCC ~ 80.0°	*anti, anti* ϕ C(O)SCC = 180.0°
LP [a] O(20) → σ* C(15)—C(16)	83.56	84.14
LP O(20) → σ* C(16)—S(28)	151.82	150.65
LP S(28) → σ* C(16)—O(20)	150.48	145.38
LP S(28) → σ* C(21)—H(22)	7.65	14.50
LP S(28) → σ* C(21)—H(23)	2.68	11.20
LP S(28) → σ* C(24)—H(26, 27)	19.94	–
LP S(28) → σ* C(21)—C(24)	16.05	–
Total	432.18	405.87

[a] LP electronic lone pair on the specific atom.

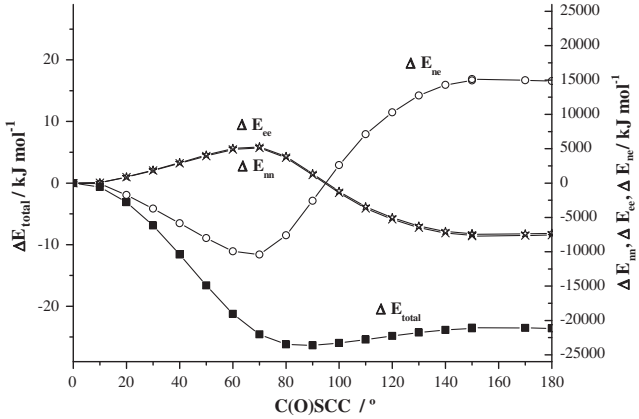

Fig. 4. Dependence of attractive (ΔE_{ne}) and repulsive (ΔE_{nn} and ΔE_{ee}) energy increments on the C(O)SCC dihedral angle in $CH_3C(O)SCH_2CH_3$, calculated at the B3LYP/6-311++G(d,p) level.

$$\Delta E = \Delta E_{nn} + \Delta E_{en} + \Delta E_{ee} + \Delta E_k \quad (2)$$

where ΔE is the total energy change between structures of different geometries, ΔE_{nn} is the energy change for nuclear repulsion, ΔE_{en} represents electron–nuclear attraction, ΔE_{ee} is electron repulsion and ΔE_k is the kinetic energy. It can be seen that this equation describes the total energy change as a sum of all potential and kinetic contributions.

Fig. 4 illustrates the fact that the repulsive terms, E_{ee} and E_{nn}, are larger in the less stable conformation than they are for the more stable C_s conformer. It can be seen that the repulsive terms, E_{ee} and E_{nn}, as functions of the torsion angle, show the same trend as V_1, which indicates that V_1 accounts for the repulsive non-bonding interactions that favor the C_s conformer stabilization.

The fact that the repulsion terms, E_{ee} and E_{nn}, are smaller in the C_s conformer than in the C_1 conformer may be explained by the great stability of: (a) the electronic lone pair, LP(1) and LP(2) on the S atom and (b) the bond orbital (σ) and antibond orbital (σ*) of the C(21)—C(24) bond in the C_s form as in the C_1 conformer. Thus the repulsive interactions between the electronic lone pair on the S atom and the charge density are lower in the C_s conformer. Table S3 shows the occupancy and NBO energies.

Vibrational analysis

The details of the IR (gas and liquid) and Raman spectra (liquid), together with a tentative assignment, are collected in Table 3. Representative spectra are illustrated in Fig. 5 (IR and Raman spectra of the liquid phase) and Fig. 6 (average calculated and experimental IR spectra).

The calculated wavenumbers for the 36 normal modes of vibration of $CH_3COSCH_2CH_3$ (22 A′ and 14 A″) for the C_s and C_1 conformers appear in Table 3, where they are compared with the measured values. The assignment of the experimental bands was made after comparison with related molecules [3,15–18] and with the results of the calculations.

Fig. 6 shows the IR spectrum conformational average. This spectrum was simulated by summing the population-weighted spectra for C_s and C_1 conformers calculated using B3LYP/6-311++G(d,p) wavenumbers and intensities with Lorenzian band shapes (γ = 2 cm^{-1}). The populations were calculated using the Boltzmann statistic for a 49% and 51% abundance of the two conformers, respectively.

Methyl and methylene group modes

One of the two antisymmetric stretching modes of the CH_3 group bonded at the C=O group was assigned to the shoulder located at 3002 cm^{-1} (gas IR) while the other was assigned to one of components of the weak band at 2981 cm^{-1} (gas IR). The latter band was assigned to the two antisymmetric stretching modes of the CH_3 group bonded at the CH_2 group, according with the

Table 3
Wavenumbers (in cm^{-1}) and observed bands in infrared and Raman spectra of $CH_3C(O)SCH_2CH_3$.

Infrared[a]		Raman[b]	Calculated IR[c]		Approximate description of mode
Gas (10 Torr.)	Liquid (R.T.)	Liquid (R.T.)	*C_s conformer*	*C_1 conformer*	
3002 sh	–		3130 (7.37)	3131 (6.94)	ν_a CH_3(CO)
2998 sh	–		3126 (14.08)	3126 (10.05)	ν_a CH_2
2988	2986 sh	2969 (30)	3109 (3.73)	3100 (3.61)	ν_a CH_3(CO)
			3096 (19.37)		
2981 w	2970 m			3106 (7.65)	ν_a $CH_3(CH_2)$
2974			3094 (15.56)	3090 (23.68)	ν_a $CH_3(CH_2)$
2950					
2944 w	2932 m	2931 (100) (C_s) 2926 (100) (C_1)	3071 (3.73)	3064 (10.11)	ν_s CH_2
2938 sh					
	2904 sh		3041 (2.36)	3041 (2.017)	ν_s CH_3(CO)
2890 vw	2875 w	2875 (21)	3032 (2905)	3029 (29.47)	ν_s $CH_3(CH_2)$
1709vs	1692 vs	1697 sh (C_1) 1689 (13) (C_s)	1756 (292.75)	1758 (261.79)	ν C=O
	1694 sh				
1710	1454	1454 (10)	1503 (4.32)	1500 (5.39)	δ_a $CH_3(CH_2)$
			1496 (9.48)	1492 (9.92)	δ_a $CH_3(CH_2)$
1458 vw		1428 sh (C_s)	1480 (4.96)		δ CH_2 (C_s)
1425 vvw	1424 sh	1424 sh	1474 (12.10)	1475 (12.23)	δ_a CH_3(CO)
			1470 (8.83)	1469 (10.10)	δ_a CH_3(CO)
	1416 m	1416 (8) (C_1)		1459 (8.12)	δ CH_2(C_1)
	1375 w	1379 (2)	1418 (3.72)	1413 (5.91)	δ_s $CH_3(CH_2)$
1364 w					
1358 w	1355 m	1354 (3)	1388 (19.25)	1388 (20.61)	δ_s CH_3(CO)
1352 sh					
	1266 m	1267 (3)	1306 (21.18)	1309 (17.3)	ω CH_2
1276					
1271 w		1252 (2)	1262 (0.061)	1287 (0.54)	τω CH_2
1266					
1141 s(C_1) 1136 s(C_s)	1134 s	1134 (3)	1124 (175.58)	1125 (160.48)	ρ CH_3(CO)
1106 w		1102 (2)			
1061 vw	1057 s	1058 (12)	1078 (2.53)	1076 (3.07)	ρ $CH_3(CH_2)$
	1047 w	1047 sh	1058 (0.05)	1070 (1.21)	ρ $CH_3(CH_2)$
1001 vw	1003 vw		1017 (2.23)	1017 (3.14)	ρ CH_3(CO)
974 sh	972 vw	974 (4)	991 (4.55)	984 (15.44)	ν CH_2—CH_3
952 m	950 s	953 (4)	976 (72.31)	972 (63.92)	ν CH_3—C(O)
764 sh	773 vw (C_s) 754 w (C_1)	752 (2)	780 (3.59)	759 (1.95)	ρ CH_2
690	678 m	689 sh (C_s) 678 (14) (C_1)	678 (3.52)	661 (13.56)	ν S—CH_2
629					
624 m	624 s	625 (59)	620 (70.31)	613 (58.26)	ν C(O)—S
618					
–	529 w	538 h	540 (1.20)	540 (1.01)	ρ C=O out of plane
		530 (4)			
–	492 vw	491 (15)	496 (0.16)	486 (0.52)	ρ C=O in plane
–	–	375 (8) (C_1) 357 (4) (C_s)	348 (1.14)	375 (1.59)	δ $SC(O)CH_3$
–	–	315 (27)	307 (2.21)	308 (3.20)	δ SCH_2CH_3
–	–	261 sh	253 (1.16)	269 (3.20)	τ CH_3 (CH_2)
–	–	–	144 (4.76)	187 (4.79)	
–	–	–	123 (4.53)	103 (3.42)	τ S—C(O)
–	–	–	35 (1.89)	61 (0.98)	τ S—(CH_2)
–	–	–	17 (0.17)	51 (1.52)	τ CH_3(CO)

[a] sh. shoulder; s. strong; w. weak; m. medium; v. very.
[b] Relative band heights in parentheses.
[c] B3LYP/6-311++G(d,p) calculation. Observed and calculated values in cm^{-1}.

theoretical calculation. The shoulder at 2904 cm^{-1} in liquid IR was assigned to the CH_3 symmetric stretching modes (bonded at the C=O group). The CH_2 symmetric stretching mode was located at 2875 cm^{-1} (liquid Raman) and the two CH_2 antisymmetric and symmetric stretching modes appeared at 2998 and 2944 cm^{-1} (gas IR), respectively. This last mode was split into two components (2931 and 2926 cm^{-1}) in the Raman spectrum, indicating the presence of two conformers.

The CH_3 and CH_2 bending modes should appear in 1500–1300 cm^{-1} region, where several bands and a shoulder are observed. The theoretical calculations predict that the $CH_3(CH_2)$ bending modes appear at higher frequencies than those for CH_3(CO) bending modes. Taking this argument into consideration, the band located at 1454 cm^{-1} is assigned to the two antisymmetric modes of $CH_3(CH_2)$ group, while the same mode of the CH_3(CO) is assigned to the shoulder located at 1424 cm^{-1} in the liquid Raman spectrum. The couple of bands located at 1375 and 1355 cm^{-1} (liquid IR) are assigned to the symmetric bending modes of the group $CH_3(CH_2)$ and CH_3(CO) respectively.

The bands at 1428 and 1416 cm^{-1} (liquid Raman) correspond to the CH_2 symmetric bending modes of the C_s and C_1 conformers, respectively, in agreement with the calculations. Therefore, the bands located at 773 and 754 cm^{-1} (liquid IR) were assigned to this mode for the C_s and C_1 conformers, respectively.

Carbonyl group modes

The C=O stretching mode is one of the most sensitive bands to the different conformations present in the compound. In the IR spectrum it appears like a broad and very intense band. In the liquid Raman spectrum this band appears at 1689 cm^{-1} and the

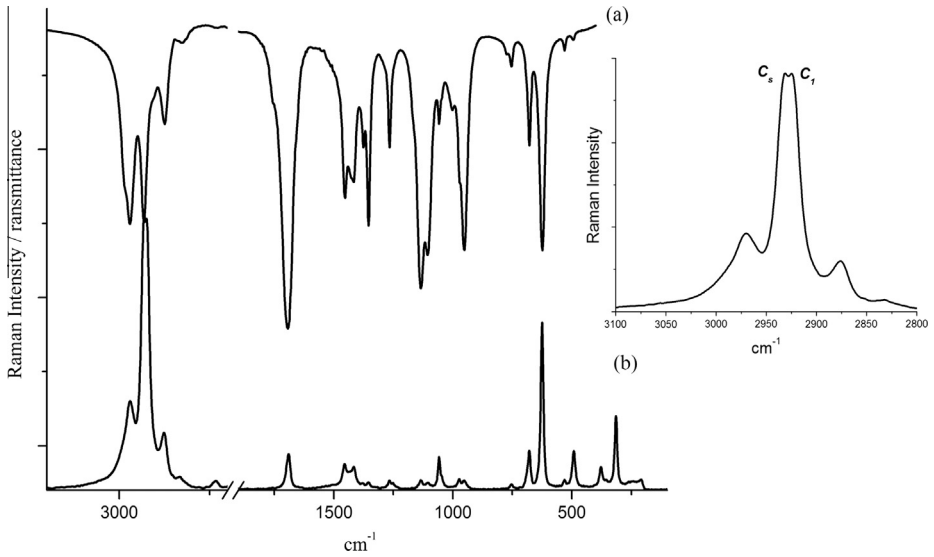

Fig. 5. Experimental spectra of $CH_3C(O)SCH_2CH_3$: Infrared (a) and Raman (resolution 2 cm^{-1}) (b) in the liquid phase. On the right is an enlargement of the Raman spectrum of the liquid phase at 3000–2800 cm^{-1} region.

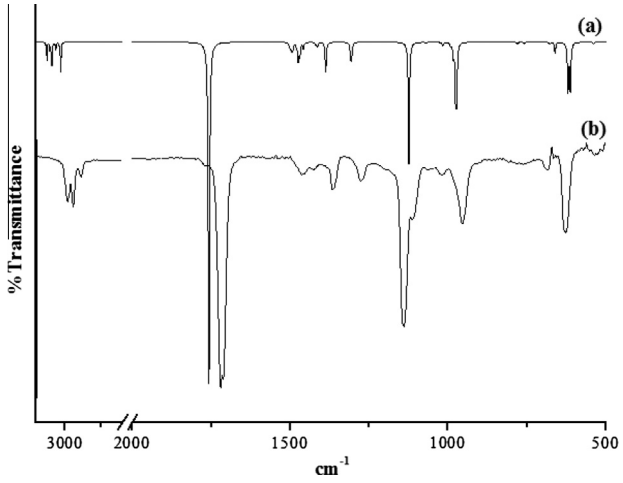

Fig. 6. Calculated (a) and experimental infrared spectra (b) (10 Torr, resol. 2 cm^{-1}) of $CH_3C(O)SCH_2CH_3$ between 3150 and 500 cm^{-1}. The calculated spectrum was obtained from B3LYP/6-311++G** frequencies and intensities using Lorentzian band shapes and populations for both conformers. The populations were calculated using the Boltzmann statistic for a 49% and 51% abundance of the two conformers, respectively.

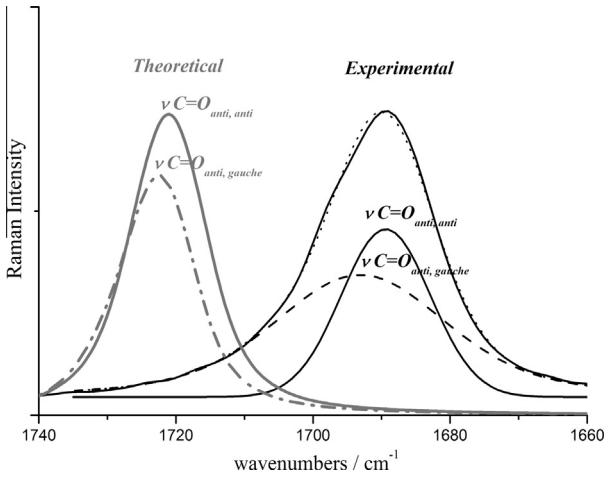

Fig. 7. Calculated spectra at B3LYP/6-311++G(d,p) to the both conformers (gray line) and deconvoluted experimental liquid Raman spectrum (black line) of the C=O stretching region to the $CH_3C(O)SCH_2CH_3$.

shoulder is seen at 1697 cm^{-1}. It was deconvoluted and compared with the bands calculated for the *anti*, *gauche* and *anti*, *anti* conformers (Fig. 7). The bands located at 530 and 491 cm^{-1} (liquid Raman) are assigned to the C=O out-of-plane and C=O in-plane wagging modes according with the calculated frequencies (539 and 489 cm^{-1}).

Skeletal modes

The shoulder at 974 cm^{-1} and the band at 952 cm^{-1} in the gas IR spectrum were associated at the CH_2—CH_3 and H_3C—C(O) stretching modes, respectively. In the liquid Raman spectrum we observed the shoulder at 689 cm^{-1} and the medium intensity band at 678 cm^{-1}. They were assigned to the CS—CH_2 stretching mode of the C_s and C_1 conformers respectively. The strong band at 625 cm^{-1} was assigned to the (O)C—S(CH_2) stretching mode. The couple of bands assigned at 375 and 357 cm^{-1} in the liquid Raman spectrum

Table 4
Population relationship between C_1 and C_s conformers of type $CX_3C(O)YCH_2CX_3$ with X = H.F e Y = O. S.

	Experimental (GED) C_1:C_s	Calculate C_1:C_s
$CF_3C(O)OCH_2CF_3$	45:55	41:59
$CF_3C(O)OCH_2CH_3$	44: 56	39: 61
$CF_3C(O)SCH_2CH_3$	49:51	41:59
$CH_3C(O)SCH_2CH_3$	–	51:49

were assigned to the H_3C—C(O)—SCH_2 bending mode of the C_1 and C_s conformers, respectively. The band located at 315 cm^{-1} in the liquid Raman spectrum was associated to the S—CH_2—CH_3 bending modes.

Comparison of conformation and vibrational properties of —C(O)S— and —C(O)O— compounds

The functional group idea is useful to understand the chemistry of biological macromolecules. Atoms and functional groups

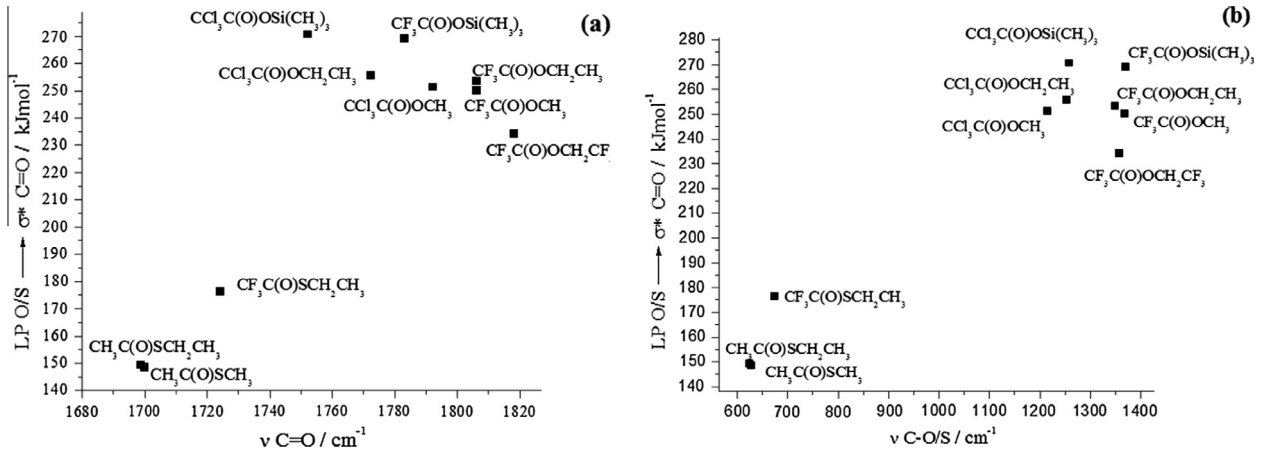

Fig. 8. Relationship between the anomeric effect LP S/O → σ*C=O: (a) ν C=O and (b) ν C—O in —C(O)S— and the —C(O)O— compound.

possess characteristic and additive properties that in many cases exhibit a remarkable transferability between different molecules. Knowledge of the structural properties and conformational preference of simple molecules containing distinct functional groups is therefore of prime interest.

In our work group we study compounds of $CX_3C(O)YCH_2CX_3$ general formula with X = H, F and Y = O, S. These compounds have two conformations: one with a C_s symmetry and another with C_1 symmetry. Their population ratios vary according to the electronegativity of the X and Y atoms. Both calculated and experimental population ratios of the two conformers of different molecules are presented in Table 4. In this table it is possible to see that when the O atom is replaced by that of S (of larger size and less electronegativity than O) at position Y, the population ratio is closer to unity.

The analysis of the potential energy barrier carried out for each of these molecules indicates that the *anti*, *anti* (C_s) conformation is favored by electrostatic interactions included in the term of Lewis and in the V_1 term of the Fourier expansion. The interactions, including hyperconjugative, conjugative and V_2, are responsible for the stabilization of the *anti*, *gauche* (C_1) form, mainly by the interaction of the electron free pair of the O or S atoms with the antibonding orbital σ^*CH_2—CH_3. The *anti*, *gauche* form is greatly stabilized by hyperconjugative interactions of the lone pairs of O (8) with the neighboring link: σ^*CF_3—C(O) and σ^*CH_2—CH_3. A simple interpretation of this phenomenon of favorable interaction of the *anti*, *gauche* form over *anti*, *anti*, could be that the interacting atoms have more positive charges in the *anti*, *gauche* form, consequently favoring electro donation from the O to the σ^*CH_2—CH_3. That is why we observe an increase in the population of this conformer when substituents are O by S or CH_2—CH_3 by CH_2—CF_3.

The behavior of hyperconjugative interactions with changing substituents and their relationship to vibrational properties is studied with the NBO program to understand how this group affects the change of substituents.

Fig. 8a presents the relationship between the anomeric effect LP S/O → σ*C=O and the νC=O in —C(O)S— and the —C(O)O— compounds. In this figure an increment can be observed in the anomeric effect LP O → σ*C=O when the ν C=O decreases. This effect being higher when the C=O group is bonded to the more electronegative group for the —C(O)O— compounds.

For —C(O)S— compounds the behavior is the opposite direction, where an increase of the LP S → σ*C=O anomeric effect increases the ν C=O.

It is important to note that the greater the difference in the electronegativity of environment, the higher is the energy interaction LP S/O → σ*C=O. Therefore, to a higher anomeric effect, a strengthening of C—O/S bond is expected, which is reflected in an increment in the stretching frequencies of this mode (Fig. 8b). These delocalization interactions are considerably higher in the oxoesters and increase the activation energy of the reaction compared to that in thioesters, being the C—S bond more likely to be broken in these compounds with the consequent S availability for an S—S type bond in biological processes.

Conclusions

The optimized molecular geometry and the conformations for $CH_3C(O)SCH_2CH_3$ have been calculated using MP2 and DFT techniques and a different basis set. The structural results show the existence of two energetically equivalent conformers.

NBO calculations were performed to explain the preferred conformation of $CH_3C(O)SCH_2CH_3$. We conclude that the electrostatic and steric contributions included in the Lewis term tend to favor the *anti*, *anti* conformer, whereas the delocalization contribution tends to favor the *anti*, *gauche* conformer, as expected from the anomeric effect.

IR and Raman spectra were obtained for $CH_3C(O)SCH_2CH_3$, for which 33 out the expected 36 normal modes of vibration are assigned. Both conformers were detected in the IR and Raman spectra.

A relationship was found between the anomeric effects LP S/O → σ*C=O and the ν C=O and the νC—O/S.

Acknowledgments

This work was supported by CIUNT-Argentina (26D-411) and CONICET (PIP 0205). M.E.D.L. is recipient of a postdoctoral fellowship from CONICET.

Appendix A. Supplementary material

Supplementary data associated with this article can be found, in the online version, at http://dx.doi.org/10.1016/j.saa.2014.07.054.

References

[1] D. Xu, K. Prasad, A. Repic, T.J. Blacklock, Tetrahedron Lett. 36 (1995) 41.
[2] A.M.M. El-Aasar, C.P. Nash, L.L. Ingraham, Biochemistry 21 (1982) 1972.
[3] C.O. Della Védova, R.M. Romano, H. Oberhammer, J. Org. Chem. 69 (2004) 5395.
[4] J.J.C. Teixeira-Dias, R. Fausto, L.A.E. Batista de Carvalho, J. Mol. Struct. (THEOCHEM) 262 (1992) 87–103.

[5] R. Fausto, P.J. Tonge, P.R. Carey, J. Chem. Soc. Faraday Trans. 90 (23) (1994) 3491–3503.
[6] W. Yang, D.G. Drueckhammer, J. Am. Chem. Soc. 123 (2001) 11004.
[7] S.E. Ulic, C.O. Della Védova, A. Hermann, H.-G. Mack, H. Oberhammer, Inorg. Chem. 41 (2002) 5699.
[8] Q. Shen, K. Hagen, J. Mol. Struct. 128 (1985) 41.
[9] R.M. Romano, C.O. Della Védova, A.J. Downs, H. Oberhammer, S. Parsons, J. Am. Chem. Soc. 123 (2001) 12623.
[10] H.-G. Mack, H. Oberhammer, C.O. Della Védova, J. Phys. Chem. 95 (1991) 4238.
[11] H.-G. Mack, C.O. Della Védova, H. Oberhammer, J. Phys. Chem. 96 (1992) 9215.
[12] S.E. Ulic, A. Kosma, C.O. Della Védova, H. Willner, H. Oberhammer, J. Phys. Chem. 110 (2006) 10201.
[13] M.F. Erben, C.O. Della Védova, H.-G. Mack, H. Oberhammer, R. Boese, Inorg. Chem. 44 (2005) 7070.
[14] A. Hermann, S.E. Ulic, C.O. Della Védova, H. Willner, H. Oberhammer, J. Fluorine Chem. 112 (2001) 297.
[15] M.E. Defonsi Lestard, M.E. Tuttolomondo, D.A. Wann, H.E. Robertson, D.W.H. Rankin, A. Ben Altabef, J. Chem. Phys. 131 (2009). 214303-1.
[16] M.E. Defonsi Lestard, M.E. Tuttolomondo, E.L. Varetti, D.A. Wann, H.E. Robertson, D.W.H. Rankin, A. Ben Altabef, J. Raman Spectrosc., J. Raman Spect. 40 (12) (2009) 2053.
[17] M.E. Defonsi Lestard, M.E. Tuttolomondo, D.A. Wann, H.E. Robertson, D.W.H. Rankin, A. Ben Altabef, J. Raman Spect. 41 (10) (2010) 1357.
[18] M.E. Defonsi Lestard, M.E. Tuttolomondo, E.L. Varetti, D.A. Wann, H.E. Robertson, D.W.H. Rankin, A. Ben Altabef, J. Mol. Struct. 917 (2009) 183.
[19] M.J. Frisch, G.W. Trucks, H.B. Schlegel, G.E. Scuseria, M.A. Robb, J.R. Cheeseman, J.A. Montgomery, Jr., T. Vreven, K.N. Kudin, J.C. Burant, J.M. Millam, S.S. Iyengar, J. Tomasi, V. Barone, B. Mennucci, M. Cossi, G. Scalmani, N. Rega, G.A. Petersson, H. Nakatsuji, M. Hada, M. Ehara, K. Toyota, R. Fukuda, J. Hasegawa, M. Ishida, T. Nakajima, Y. Honda, O. Kitao, H. Nakai, M. Klene, X. Li, J.E. Knox, H.P. Hratchian, J.B. Cross, C. Adamo, J. Jaramillo, R. Gomperts, R.E. Stratmann, O. Yazyev, A.J. Austin, R. Cammi, C. Pomelli, J.W. Ochterski, P.Y. Ayala, K. Morokuma, G.A. Voth, P. Salvador, J.J. Dannenberg, V.G. Zakrzewski, S. Dapprich, A.D. Daniels, M.C. Strain, O. Farkas, D.K. Malick, A.D. Rabuck, K. Raghavachari, J.B. Foresman, J.V. Ortiz, Q. Cui, A.G. Baboul, S. Clifford, J. Cioslowski, B.B. Stefanov, G. Liu, A. Liashenko, P. Piskorz, I. Komaromi, R.L. Martin, D.J. Fox, T. Keith, M.A. Al-Laham, C.Y. Peng, A. Nanayakkara, M. Challacombe, P.M.W. Gill, B. Johnson, W. Chen, M.W. Wong, C. Gonzalez, J.A. Pople, Gaussian 03, Revision D.01; Gaussian Inc., Wallingford, CT, 2004.
[20] C. Møller, M.S. Plesset, Phys. Rev. 46 (1934) 618–622.
[21] J.P. Perdew, K. Burke, M. Ernzerhof, Phys. Rev. Lett. 77 (1996) 3865–3868. Erratum: Phys. Rev. Lett. 78 (1997) 1396.
[22] D. Becke, J. Chem. Phys. 98 (1993) 5648–5652.
[23] C. Lee, W. Yang, R.G. Parr, Phys. Rev. B 37 (1988) 785–789.
[24] E.D. Glendening, J.K. Badenhoop, A.D. Reed, J.E. Carpenter, F.F. Weinhold, Theoretical Chemistry Institute, University of Wisconsin, Madison, WI, 1996.
[25] M.E. Tuttolomondo, A. Navarro, T.P.E. Peña, E.L. Varetti, S.A. Hayes, D.A. Wann, H.E. Robertson, D.W.H. Rankin, A. Ben Altabef, J. Phys. Chem. A 111 (2007) 9952.
[26] M.E. Defonsi Lestard, L.A. Ramos, M.E. Tuttolomondo, S.E. Ulic, A. Ben Altabef, Vibrat. Spectrosc. 59 (2012) 40.
[27] M.E. Defonsi Lestard, L.A. Ramos, M.E. Tuttolomondo, S.E. Ulic, A. Ben Altabef, Spectrochim. Acta, Part A: Mol. Biomol. Spectrosc. 96 (2012) 332.
[28] A.D. McLean, G.S. Chandler, J. Chem. Phys. 72 (1980) 5639.
[29] M.J. Frisch, J.A. Pople, J.S. Binkley, J. Chem. Phys. 80 (1984) 3265.
[30] W.J. Hehre, P.v.R. Schleyer, J.A. Pople, Ab initio Molecular Orbital Theory, Wiley, New York, 1986.
[31] L. Radom, J.A. Pople, J. Am. Chem. Soc. 92 (1970) 4786.
[32] L. Radom, W.J. Hehre, J.A. Pople, J. Am. Chem. Soc. 94 (1972) 2371.
[33] D. Douglas, P.v.R. Schleyer, J. Org. Chem. 55 (1990) 1003.
[34] S. Millefiori, A.J. Alparone, Chem. Soc. Faraday Trans. 94 (1998) 25.